

Infrared-to-Visible Up-conversion in Er-Pr-Yb Triply Doped Oxyfluoride Glass Ceramics

Su-A Song¹ and Ki-Soo Lim^{2*}

¹Department of Aerospace Engineering, Korea Aerospace University, Goyang 10540, Korea

²Department of Physics, Chungbuk National University, Cheongju 28644, Korea

(Received August 30, 2016 : revised October 17, 2016 : accepted November 29, 2016)

We synthesized Er³⁺-Yb³⁺, Pr³⁺-Yb³⁺, and Er³⁺-Pr³⁺-Yb³⁺ -doped oxyfluoride glass ceramics containing CaF₂ nanocrystals by proper thermal treatments. Spectral characteristics of down- and up-converted emissions in three kinds of glass ceramics under 365-nm and 980-nm excitations were compared and explained by cross relaxations, excited-state absorptions, and energy-transfer processes between different ions. The huge reduction of up-conversion emission in the triply doped glass ceramics under 980-nm excitation compared to the Er³⁺-Yb³⁺ codoped one was explained by the split pump power and the direct energy transfer from Er³⁺ to Pr³⁺ ions. Increasing Yb³⁺ concentration from 2% to 10% in the triply doped glass ceramics showed more than quadratic enhancement of the absorbed power, and we explained it by the enhanced energy-transfer efficiency from Yb³⁺ to Er³⁺ ions. We also observed enhanced up-converted emissions of Er³⁺ and Pr³⁺ ions in three kinds of glass ceramics under simultaneous excitation at 980 nm and 1550 nm, and suggested detailed up-conversion mechanisms.

Keywords : Glass ceramics, Er, Pr, Yb, Up-conversion

OCIS codes : (160.2540) Fluorescent and luminescent materials; (160.2750) Glass and other amorphous materials; (160.4236) Nanomaterials; (160.5690) Rare-earth-doped materials; (190.7220) Upconversion

I. INTRODUCTION

Up-conversion materials doped with rare-earth ions have been a significant interest in recent years due to various potential applications, such as biological labeling, three-dimensional displays, solar cells, etc. [1-3]. Oxyfluoride glass ceramics have been widely investigated as host materials for rare-earth ions recently, because they have the advantages of not only low phonon energies but also high chemical and mechanical stabilities [4]. CaF₂ is a nontoxic optical material with a wide spectral region of transparency, high solubility of rare-earth ions [5], and a good match of refractive index with aluminosilicate glass [6]. Doped rare-earth ions are confined in CaF₂ nanocrystals with much less phonon energy, yielding large quantum efficiency [7]. A solar-cell material with a high band gap, such as amorphous silicon, loses the near-infrared

portion of the solar spectrum, above 730 nm, but multiply doped systems may improve up-conversion characteristics, because a rare-earth ion has many absorption levels in the near-infrared. Most previous studies on up-conversion processes have been reported for singly or doubly doped materials. Er³⁺ ions showing green and red up-conversion emissions are known as the most efficient up-conversion activators [8], and Pr³⁺ ions have many energy levels close to those of Er³⁺ ions, enabling energy transfer between these two species. Yb³⁺ ions are well-known sensitizers that have a high absorption cross section around 980 nm and transfer energy efficiently to Er³⁺ or Pr³⁺ ions [9, 10].

There have been only a few investigations of triply doped glass ceramics. The up-conversion properties of a system triply doped with Er³⁺, Pr³⁺, and Yb³⁺ was only investigated in tellurite glass, as far as we know [11]. In the present study, we

*Corresponding author: kslim@chungbuk.ac.kr

Color versions of one or more of the figures in this paper are available online.



This is an Open Access article distributed under the terms of the Creative Commons Attribution Non-Commercial License (<http://creativecommons.org/licenses/by-nc/3.0/>) which permits unrestricted non-commercial use, distribution, and reproduction in any medium, provided the original work is properly cited.

report the infrared-to-visible up-conversion energy transfers in Er^{3+} , Pr^{3+} , and Yb^{3+} triply doped transparent glass ceramics containing CaF_2 nanocrystals, and compare the results to those in double doped systems under excitation at 980 nm. We also compare the up-conversion emissions of triply doped glass ceramics under excitation at 980 nm to those under simultaneous excitations at 980 and 1550 nm.

II. EXPERIMENTAL

Oxyfluoride glass hosts were prepared with the composition (in mol%) $45\text{SiO}_2\text{-}22\text{Al}_2\text{O}_3\text{-}11\text{CaO-}22\text{CaF}_2$. Dopants were 1%Er-2%Yb (ErYb), 1%Pr-2%Yb (PrYb), 1%Er-1%Pr-2%Yb (ErPrYb), and 1%Er-1%Pr-10%Yb (ErPrYb(10)). For each batch, the raw material was mixed and melted in a covered platinum crucible in air at 1400°C for 1 h, and then cast into an iron mold, followed by annealing at 530°C for 10 h to release the inner stress. The temperatures of the glass transition temperature and the onset of crystallization were measured by differential thermal analysis (DTA, SDT2960). The glass samples were then annealed precisely at 760°C for 4 h to induce crystallization, and polished for optical measurements. Oxyfluoride precursor glass and glass ceramic samples are denoted as G and GC respectively. We confirmed the formation of CaF_2 crystal phases by x-ray diffraction (XRD, RIGAKU, SmartLab) analysis. The up-conversion and down-conversion luminescences were measured with a monochromator (DK240) and photomultiplier tube (PMT) under diode-laser excitations at 365, 980, and 1550 nm.

III. RESULTS AND DISCUSSION

Figure 1 shows the XRD patterns of triply doped samples.

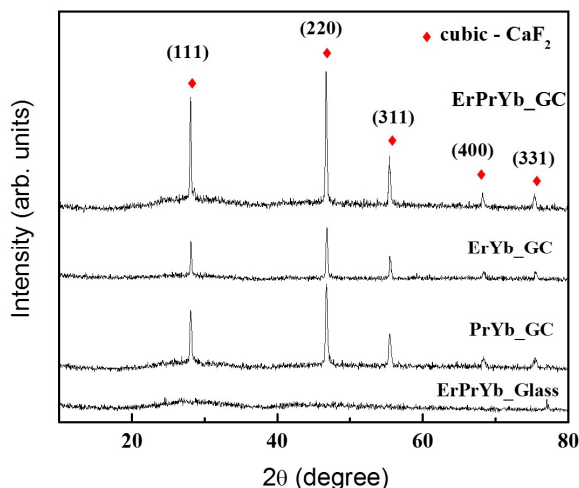


FIG. 1. XRD patterns of ErPrYb_GC, ErYb_GC, PrYb_GC, and ErPrYb_Glass.

The ErPrYb_G shows broad humps due to the amorphous structure. The background patterns of the ErYb_GC, PrYb_GC, and ErPrYb_GC treated at 760°C show peaks easily assigned to cubic CaF_2 (JCPDS 35-0816). We estimate the average nanocrystal size as 40-50 nm from XRD line-broadening measurements, using Sherrer's equation [12],

$$D(hkl) = \frac{K\lambda}{\beta \cos\theta} \quad (1)$$

where $D(hkl)$ is the crystal size in the direction (hkl) , λ is the wavelength of the x-rays, θ is the angle of diffraction, β is the full width at half maximum (FWHM) of the diffraction peak, and K is the instrument's constant (0.9). The absorption spectrum of the glass reveals three kinds of dopants, as shown in Fig. 2. All three ions have absorptions at 980 nm.

The down-conversion spectra of the ErYb_GC, PrYb_GC, and ErPrYb_GC under excitation at 365 nm showed emissions tens of times stronger than those of the glasses with the same dopants, as shown in Fig. 3. The enhancement can

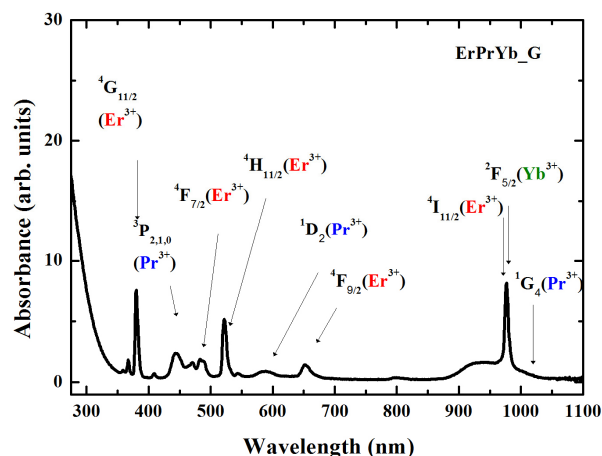


FIG. 2. Absorption spectrum of ErPrYb_Glass.

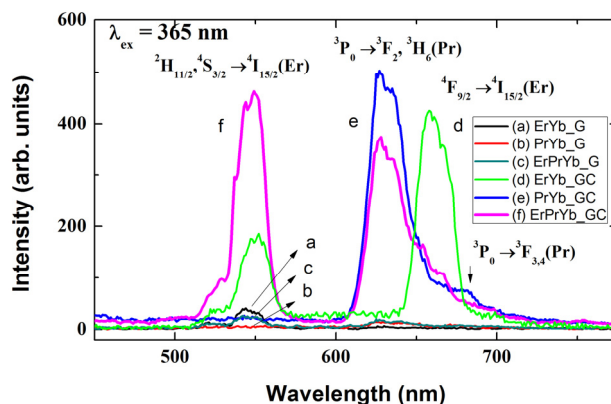


FIG. 3. Down-conversion emission spectra of ErPrYb_GC, ErYb_GC, PrYb_GC, ErPrYb_G, ErYb_G, and PrYb_G, upon 365-nm excitation.

be attributed to suppressed nonradiative relaxation of rare-earth ions incorporated into CaF_2 nanocrystals with very low phonon energy [13]. Besides, the structured spectral shape showing Stark levels in the green and red emissions indicates that Er^{3+} and Pr^{3+} ions are mainly located in crystalline domains, rather than glass domains, of the glass ceramics. In addition, the energy transfer among neighboring rare-earth ions inside CaF_2 nanocrystals can occur effectively [14], because rare-earth ions reside preferentially inside the nanocrystals rather than in the glass matrix. [15].

The spectrum of Pr^{3+} ions in glass is known to feature very broad emission in the region of 580-720 nm [16]. Our PrYb_GC also shows a broad red emission from Pr^{3+} ions, indicating the $^3\text{P}_0 \rightarrow ^3\text{H}_6$, $^3\text{F}_2$ transitions. As we can see in Fig. 3, ErYb_G has negligible red emission, because the $^4\text{F}_{9/2}$ level is populated nonradiatively from the $^4\text{S}_{3/2}$ state, and its emission cross section is smaller than that of $^4\text{S}_{3/2}$ [17]. However, in ErYb_GC , the green emission of the $^2\text{H}_{11/2}$, $^4\text{S}_{3/2} \rightarrow ^4\text{I}_{15/2}$ transitions in the region of 520-560 nm and the red emissions of the $^4\text{F}_{9/2} \rightarrow ^4\text{I}_{15/2}$ transitions show much enhancement, indicating effective energy transfer from the charge-transfer band to the high-energy states of Er^{3+} ions incorporated in CaF_2 nanocrystals. Furthermore, the red emission is stronger than the green. The $^4\text{F}_{9/2}$ emitting state can be also populated by the two cross relaxations ($^4\text{I}_{11/2} \rightarrow ^4\text{I}_{15/2}$ and $^4\text{I}_{13/2} \rightarrow ^4\text{F}_{9/2}$) and ($^4\text{F}_{7/2} \rightarrow ^4\text{F}_{9/2}$ and $^4\text{I}_{11/2} \rightarrow ^4\text{F}_{9/2}$). Besides, there can be energy transfer from Er^{3+} to Yb^{3+} ions via the $^4\text{I}_{11/2} \rightarrow ^4\text{I}_{15/2}$ (Er^{3+}) and $^2\text{F}_{7/2} \rightarrow ^2\text{F}_{5/2}$ (Yb^{3+}) transitions. Following the back-transfer process to Er^{3+} ions by the $^4\text{I}_{13/2} \rightarrow ^4\text{I}_{9/2}$ (Er^{3+}) and $^2\text{F}_{5/2} \rightarrow ^2\text{F}_{7/2}$ (Yb^{3+}) transitions can enhance the red emission.

ErPrYb_GC shows strong green (Er^{3+}) and red (Pr^{3+}) emissions. However, the red emission of the Pr^{3+} ions is much reduced. The spectral shapes of the PrYb_GC and ErPrYb_GC are similar, but the difference of two normalized spectra clearly shows only a purely red emission band of Er^{3+} ions at 660 nm. Very effective energy transfer of the $^4\text{I}_{13/2}$ (Er^{3+}) \rightarrow $^3\text{F}_{3,4}$ (Pr^{3+}) and $^4\text{I}_{11/2}$ (Er^{3+}) \rightarrow $^1\text{G}_4$ (Pr^{3+}) channels reduces the populations of the $^4\text{I}_{13/2}$ and $^4\text{I}_{11/2}$ states of the Er^{3+} ions. The resultant inactivity of the two cross relaxations that are effective in ErYb_GC produces weak red emission from the $^4\text{F}_{9/2}$ state [18-20].

Besides, the excitation energy at 365 nm is split between the Er^{3+} and Pr^{3+} ions, and the $^4\text{I}_{11/2} \rightarrow ^4\text{I}_{15/2}$ transition energy of the Er^{3+} is transferred not only to Yb^{3+} ($^2\text{F}_{7/2} \rightarrow ^2\text{F}_{5/2}$) but also to Pr^{3+} ($^3\text{H}_4 \rightarrow ^1\text{G}_4$). Furthermore, the excited energy of the $^2\text{F}_{5/2}$ state (Yb^{3+}) can be transferred to both Er^{3+} and Pr^{3+} ions. Those processes result in the greatly reduced red emission of Er^{3+} ions in ErPrYb_GC . In contrast, the effective energy transfer from Pr^{3+} ($^3\text{P}_0$) to Er^{3+} ($^4\text{F}_{7/2}$) ions [21] contribute to the increasing green emission of Er^{3+} ions in ErPrYb_GC .

The up-converted emission spectra of ErYb_GC , PrYb_GC , ErPrYb_GC , and ErPrYb(10)_GC excited at 980 nm are shown in Fig. 4. Pr^{3+} ions showed little absorption at 980 nm, because the oscillator strength of the $^1\text{G}_4$ state has its

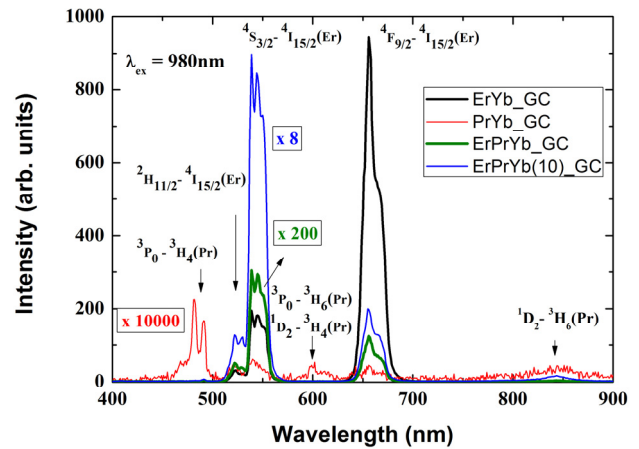


FIG. 4. Up-conversion emission spectra of ErPrYb_GC , ErYb_GC , PrYb_GC , and ErPrYb(10)_GC , upon 980-nm excitation.

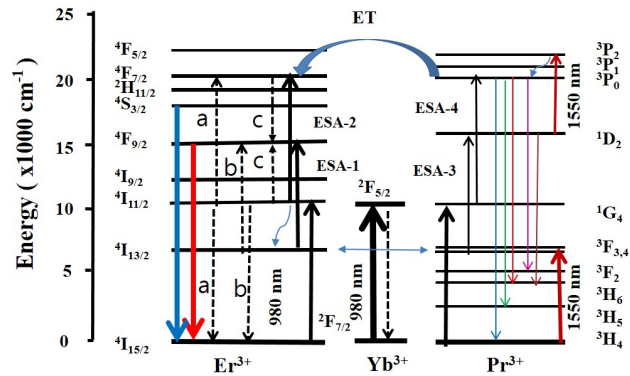


FIG. 5. Partial energy-level diagram of ErPrYb_GC and up-conversion mechanisms, under excitation at 980 nm or 980 + 1550 nm.

maximum at 1020 nm. However, Er^{3+} has a weak absorption band at 980 nm, and Yb^{3+} has much stronger absorption at this wavelength, because of high oscillator strength [22] and concentration. The up-conversion emission intensity of Er -doped CaF_2 was reported to be more than an order of magnitude weaker than that of Er - Yb codoped CaF_2 under 980 nm excitation [23]. In general, efficient energy transfer occurs in Er^{3+} - Yb^{3+} codoped materials, owing to the large spectra overlap of both absorption and emission between these ions around 980 nm. The up-conversion mechanisms for green and red emissions of Er^{3+} in Er^{3+} and Yb^{3+} codoped materials are well known [9], and are described in Fig. 5. Two excited-state absorptions, the ESA-1 ($^4\text{I}_{13/2} \rightarrow ^4\text{F}_{9/2}$) and ESA-2 ($^4\text{I}_{11/2} \rightarrow ^4\text{F}_{7/2}$) transitions, are enabled by the pump energy at 980 nm, and are responsible for the red and green emissions respectively. Besides, the cross relaxation (CR)-a of ($^4\text{I}_{11/2} \rightarrow ^4\text{F}_{7/2}$) and ($^4\text{I}_{11/2} \rightarrow ^4\text{I}_{15/2}$) populates the $^4\text{F}_{7/2}$ state, and the CR-b of ($^4\text{I}_{13/2} \rightarrow ^4\text{F}_{9/2}$) and ($^4\text{I}_{11/2} \rightarrow ^4\text{I}_{15/2}$) populates the $^4\text{F}_{9/2}$ state respectively. We expect relatively stronger red emission than green because the metastable

$^4I_{13/2}$ state enables CR-b more than CR-a to increase the population of the $^4F_{9/2}$ state effectively. This reduced ratio of green:red is also driven by depopulation of the $^4F_{7/2}$ state and population of the $^4F_{9/2}$ by the CR-c of ($^4F_{7/2} \rightarrow ^4F_{9/2}$) and ($^4I_{11/2} \rightarrow ^4F_{9/2}$). However, the contribution of CR-c is relatively small, due to nonradiative relaxation from $^4F_{7/2}$ to $^2H_{11/2}$, although the CR-c process in Er-Yb codoped phosphors has been reported [24, 25].

The emission intensity from the PrYb_GC is weak, $\sim 10^{-5}$ times as strong as that from the ErYb_GC in Fig. 4. The emission bands at 480, 490, 525, 540, 600, 610, 640, 656, and 850 nm are attributed respectively to the $^3P_1 \rightarrow ^3H_4$, $^3P_0 \rightarrow ^3H_4$, $^3P_1 \rightarrow ^3H_5$, $^3P_0 \rightarrow ^3H_5$, $^1D_2 \rightarrow ^3H_4$, $^3P_0 \rightarrow ^3H_6$, $^3P_1 \rightarrow ^3F_2$, $^3P_0 \rightarrow ^3F_2$, and $^3P_1 \rightarrow ^1G_4$ transitions of Pr^{3+} [26]. The proposed up-conversion mechanism for the emissions of Pr^{3+} is also displayed in Fig. 5. The energy of excited Yb^{3+} is transferred to Pr^{3+} by ($^2F_{5/2} \rightarrow ^2F_{7/2}$) (Yb^{3+}) and ($^3H_4 \rightarrow ^1G_4$) (Pr^{3+}). The subsequent processes for Pr^{3+} are ESA-3 ($^3F_{3,4} \rightarrow ^1D_2$) and ESA-4 ($^1G_4 \rightarrow ^3P_0$). However, energy transfer from Yb^{3+} to Pr^{3+} ions is less efficient than that from Yb^{3+} to Er^{3+} [27] at 980 nm, resulting in weak visible emission from Pr^{3+} .

The ErPrYb_GC shows significant, yet weaker by a factor of over 400, up-conversion emission than the ErYb_GC, under 16-mW excitation at 980 nm. In the ErPrYb_GC, pump energy is mainly shared by Er^{3+} and Yb^{3+} ions, and their excitation energies are transferred to each other via $Yb^{3+}-Er^{3+}$ [9], $Er^{3+}-Pr^{3+}$ [19, 21], and $Yb^{3+}-Pr^{3+}$ [27] interactions.

Reduced energy transfer from Yb^{3+} to Er^{3+} in ErPrYb_GC, due to another transfer channel from Yb^{3+} to Pr^{3+} [27], weakens the ESA-1 and ESA-2 processes of Er^{3+} . Besides, as mentioned, for down-conversion in ErPrYb_GC under 365-nm excitation, two efficient energy-transfer channels from Er^{3+} to Pr^{3+} ions [18], $^4I_{13/2}(Er^{3+}) + ^3H_4(Pr^{3+}) \rightarrow ^4I_{15/2}(Er^{3+}) + ^3F_{3,4}(Pr^{3+})$ and $^4I_{11/2}(Er^{3+}) + ^3H_4(Pr^{3+}) \rightarrow ^4I_{15/2}(Er^{3+}) + ^1G_4(Pr^{3+})$, make the ESA-1 and ESA-2 processes negligible. As we can see from the spectrum of PrYb_GC in Fig. 4, Pr^{3+} ions are not effective at producing up-conversion emission under 980-nm excitation. Thus, both green and red up-conversion emissions from ErPrYb_GC are dramatically reduced.

However, the ratio of green:red emission of ErPrYb_GC is 10 times as large as that of ErYb_GC, which differs from the down-conversion seen in Fig. 3. The increased ratio of green:red emission in ErPrYb_GC can be explained mainly by suppression of the CR-b and ESA-1 processes, because of the reduced population of $^4I_{13/2}$ due to energy transfer from Er^{3+} ($^4I_{13/2}$) to Pr^{3+} ($^3F_{3,4}$) [19]. In addition, the population of the 1G_4 state (Pr^{3+}) can be increased by energy transfer from Yb^{3+} ($^2F_{5/2}$) and Er^{3+} ($^4I_{11/2}$). The probability of energy transfer from the $^4I_{9/2}$ or $^4F_{9/2}$ state of Er^{3+} is very low, because the large energy differences of those states from 1G_4 (Pr^{3+}) require many phonons to be involved. Increased population of the 1G_4 state enables the ESA-4 process to populate the 3P_0 (Pr^{3+}) state, followed by energy transfer from it to the $^4F_{7/2}$ (Er^{3+}) state [21], resulting in enhanced green emission. Thus, the ratio of green:red emission can be enhanced.

Figure 4 also shows that the green (540 nm), red (656 nm), and near-infrared (850 nm) emissions of ErPrYb(10)_GC with 10 mol% Yb^{3+} ions respectively increase by factors of 90, 40, and 150 compared to those of ErPrYb_GC with 2 mol% Yb^{3+} ions. Our up-conversion emission in the green and red regions showed no line broadening, even in 2%Er³⁺-10%Yb³⁺ codoped glass ceramics, indicating no additional inhomogeneous broadening caused by a doping concentration five times as high.

The huge enhancement seen just by increasing Yb^{3+} concentration by a factor of 5 is not easily understood. Moreover, in ErPrYb(10)_GC the ratio of green:red emission is improved more than twofold. Chen *et al.* [9] reported that the ratio of green:red emission in the ErYb system decreases with Yb^{3+} concentration, down to almost zero for 10% Yb^{3+} concentration, under 980-nm excitation in codoped ZrO₂ nanocrystals. The ratio of green:red emission for ErYb_GC in Fig. 4 is twice as large as in their report, for the 1%Er-2%Yb system. The Stark-splitting levels of Er^{3+} and Pr^{3+} are revealed in the emission bands, indicating that Er^{3+} and Pr^{3+} ions are located in the crystalline phase.

The up-conversion channels in ErPrYb(10)_GC are assumed to be about the same as in ErPrYb_GC. The huge enhancement of two emissions are ascribed to electrons accumulating in the $^2F_{5/2}$ state of highly concentrated Yb^{3+} ions, which are energy providers and intermediates, because they do not have any excited state in the visible except for $^2F_{5/2}$.

In general, Yb^{3+} ions have been reported as proper dopants for up-conversion, with concentrations as high as 10-25 mol% in materials such as CaF₂ [28], PbF₂ [29], and NaLuF₄ crystals [30], without concentration quenching under 980-nm excitation. The emission intensity is proportional to I^n , where I is excitation intensity and n is the number of pump photons required.

The power dependence of the green and red emissions of ErPrYb_GC is shown in Fig. 6. The slope of 2.1 for the red emission implies that it originates mainly from a two-photon process, in the present power range. The slope of 2.3 for the green emission suggests that it has not only the two-photon channel of $^4I_{15/2} \rightarrow ^4I_{11/2}$ and ESA-2, but also the three-photon channel of $^4I_{15/2} \rightarrow ^4I_{11/2}$, ESA-1, and ESA-2 transitions, including nonradiative relaxations [31]. Energy transfer from the 3P_0 (Pr^{3+}) to $^4F_{7/2}$ (Er^{3+}) states follows another three-photon channel, consisting of the $^3H_4 \rightarrow ^1G_4$, ESA-3, and ESA-4 transitions [21]. Thus the slope of the green emission is less than 3.

Increasing the concentration of Yb^{3+} ions from 2% to 10% corresponds to a fivefold increase in absorption at 980 nm. The factor of 70 enhancement in up-conversion intensity seen in Fig. 6 may be explained by a more than quadratic dependence on the absorbed power. Moreover, we expect more efficient energy transfer from Yb^{3+} to Er^{3+} ions at higher concentrations in CaF₂, because the average distance between Yb^{3+} and Er^{3+} ions is reduced, and the rate of energy transfer between ions is increased [32].

Excitation at 1550 nm for Pr_GC, ErPr_GC, PrYb_GC,

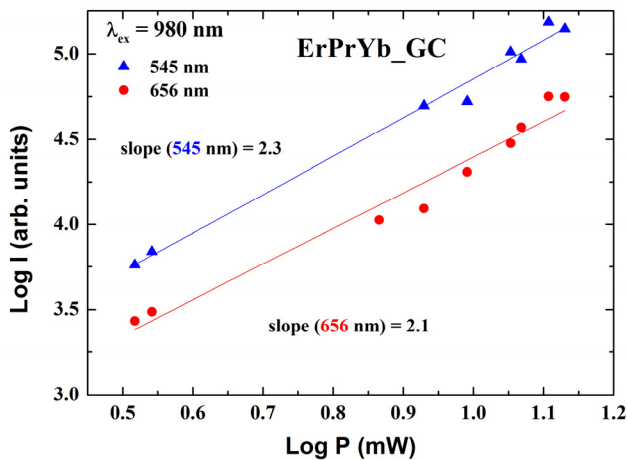


FIG. 6. Log-log plot of the power dependence of the green (545 nm) and red (656 nm) up-conversion intensities for ErPrYb_GC, upon 980-nm excitation.

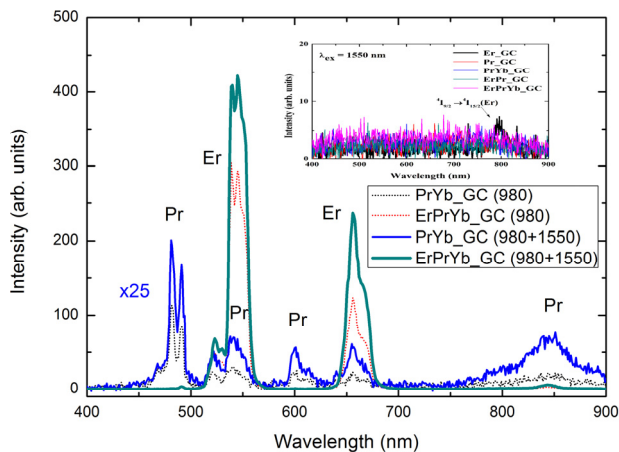


FIG. 7. Up-conversion emission spectra of ErPrYb_GC and PrYb_GC upon single excitation at 980 nm, and dual excitation at 980 and 1550 nm.

and ErPrYb_GC did not show any visible up-conversion emission. However, upon double excitation at both 980 nm (16 mW) and 1550 nm (8 mW), the ErPrYb_GC showed enhanced emissions from both Er³⁺ and Pr³⁺ ions, compared to those under single excitation at 980 nm, as shown in Fig. 7. The enhancement is assumed to originate from GSA (³H₄→³F_{3,4}) and ESA (¹D₂→³P₂) processes of 1550 nm excitation of Pr³⁺, as shown in Fig. 6. The relatively large enhancement of 850-nm emission (¹D₂→³H₆) in PrYb_GC under double excitation may be due to a more populated ¹D₂ state, thanks to ³H₄→³F_{3,4} and ESA-3 transitions.

IV. CONCLUSIONS

In down-conversion emission under excitation at 365 nm, two cross relaxations of (⁴I_{11/2}→⁴I_{15/2} and ⁴I_{13/2}→⁴F_{9/2})

and (⁴F_{7/2}→⁴F_{9/2} and ⁴I_{11/2}→⁴F_{9/2}) in ErYb_GC decreased the ratio of green:red emission of Er³⁺ ions. In contrast, the inactivity of two cross relaxations in ErPrYb_GC, due to energy transfer from Er³⁺ to Pr³⁺, increased the ratio. In up-conversion emission under 16-mW excitation at 980 nm, the strong up-conversion emission seen in ErYb_GC was reduced by more than a factor of 400 in ErPrYb_GC. This reduction was explained by diminished energy transfer from Yb³⁺ to Er³⁺, because of an additional energy-transfer channel from Yb³⁺ to Pr³⁺, on top of the direct energy transfer from Er³⁺ to Pr³⁺. Energy transfer from Pr³⁺(³P₀) to Er³⁺(⁴F_{7/2}) contributes to an increase in the green:red emission ratio. A huge enhancement of up-conversion intensity by increasing Yb³⁺ concentration fivefold was explained by quadratic dependence on the absorbed power plus enhanced efficiency in energy transfer from Yb³⁺ to Er³⁺, due to reduced Er³⁺-Yb³⁺ distance. We also compared the up-conversion emission of excitation at 980 nm to those of simultaneous excitations at 980 nm and 1550 nm in triply doped glass ceramics, and detailed up-conversion mechanisms were suggested, based on the observations.

ACKNOWLEDGMENT

This research was supported by the Basic Science Research Program through the National Research Foundation of Korea (NRF), funded by the Ministry of Science, ICT and Future Planning (2013R1A1A2007224).

REFERENCES

1. F. Wang, D. Banerjee, Y. Liu, X. Chen, and X. Liu, "Upconversion nanoparticles in biological labeling, imaging, and therapy," *Analyst* **135**, 1839-1854 (2010).
2. T. R. Hinklin, S. C. Rand, and R. M. Laine, "Transparent, polycrystalline upconverting nanoceramics: towards 3-D displays," *Adv. Mater.* **20**, 1-4 (2008).
3. S. Ivanova and F. Pellé, "Evaluating upconversion materials developed to improve the efficiency of solar cells: reply to comment," *J. Opt. Soc. Am. B* **27**, 1356-1358 (2010).
4. Y. Wang and J. Ohwaki, "New transparent vitroceraics codoped with Er³⁺ and Yb³⁺ for efficient frequency upconversion," *Appl. Phys. Lett.* **63**, 3268-3270 (1993).
5. A. J. Stevenson, H. S.-Brault, P. Gredin, and M. Mortier, "Fluoride materials for optical applications: single crystals, ceramics, glasses, and glass-ceramics," *J. Fluorine Chem.* **132**, 1165-1173 (2011).
6. X. Qiao, X. Fan, J. Wang, and M. Wang, "Luminescence behavior of Er³⁺ ions in glass-ceramics containing CaF₂ nanocrystals," *J. Non-Cryst. Solids* **351**, 357-363 (2005).
7. J. P. Srivastava and R. D. Singh, "Infrared lattice vibrational spectrum of CaF₂," *J. Phys. C: Solid State Phys.* **4**, L47-49 (1971).
8. X. Zhang, X. Wang, Y. Qiao, and H. Guo, "Synthesis and photoluminescent properties of Gd₅O₄Br:Er³⁺ phosphors prepared

- by solid-state reaction method,” *Opt. Mater.* **32**, 216-220 (2009).
9. G. Chen, G. Somesfalean, Y. Liu, Z. Zhang, and Q. Sun, F. Wang, “Upconversion mechanism for two-color emission in rare-earth-ion-doped ZrO₂ nanocrystals,” *Phys. Rev. B* **75**, 195204 (2007).
 10. C. Ming, F. Song, and L. Yan, “Spectroscopic study and green upconversion of Pr³⁺/Yb³⁺-codoped NaY(WO₄)₂ crystal,” *Opt. Commun.* **286**, 217-220 (2013).
 11. Y. Dwivedi, A. Rai, and S. B. Rai, “Intense white upconversion emission in Pr/Er/Yb codoped tellurite glass,” *J. Appl. Phys.* **104**, 043509 (2008).
 12. H. P. Klug and L. E. Alexander, *X-ray Diffraction Procedures*, 2nd ed. (Wiley, New York, USA, 1974).
 13. J. Tua, S. A. FitzGerald, J. A. Campbell, and A. J. Sievers, “Glass-like properties observed in low-frequency Raman scattering of mixed fluorite crystals,” *J. Non-Cryst. Solids* **203**, 153-158 (1996).
 14. S. A. Song, D. S. Kim, H. M. Jeong, and K. S. Lim, “Upconversion in Nd-Tm-Yb triply doped oxyfluoride glass-ceramics containing CaF₂ nanocrystals,” *J. Lumin.* **152**, 75-78 (2014).
 15. W. J. Park, C. Liu, and J. Heo, “Direct imaging of the distribution of Nd³⁺ ions in glasses containing PbS quantum dots,” *J. Am. Ceram. Soc.* **98**, 2074-2077 (2015).
 16. M. Rozanski, K. Wisniewski, J. Szatkowski, C. Koepke, M. Sroda, “Effect of thermal treatment on excited state spectroscopy of oxyfluoride borosilicate glass activated by Pr³⁺ ions,” *Opt. Mater.* **31**, 548-553 (2009).
 17. A. Lupei, V. Lupei, C. Gheorghie, and A. Ikesue, “Excited states dynamics of Er³⁺ in Sc₂O₃ ceramic,” *J. Lumin.* **128**, 918-920 (2008).
 18. S. H. Park, D. C. Lee, J. Heo, and D. W. Shin, “Energy transfer between Er³⁺ and Pr³⁺ in chalcogenide glasses for dual-wavelength fiber-optic amplifiers,” *J. Appl. Phys.* **91**, 9072-9077 (2002).
 19. Gongxun Bai, J. D., Lili Tao, Kefeng Li, Lili Hu, Yuen H. Tsang, “Efficient 2.7 micron emission from Er³⁺/Pr³⁺ codoped oxyfluorotellurite glass,” *J. Non-Cryst. Solids* **358**, 3403-3406 (2012).
 20. D. J. Coleman, P. Golding, and T. A. King, “Spectroscopic and energy-transfer parameters for Er³⁺-doped and Er³⁺, Pr³⁺-codoped GeGaS glasses,” *J. Opt. Soc. Am.* **19**, 1982-1989 (2002).
 21. F. Zhang, Z. Bi, A. Huang, and Z. Xiao, “Visible luminescence properties of Er³⁺/Pr³⁺ codoped fluorotellurite glasses,” *Opt. Mater.* **41**, 112-115 (2015).
 22. M. P. Hehlen, N. J. Cockroft, T. R. Gosnell, and A. J. Bruce, “Spectroscopic properties of Er³⁺ and Yb³⁺ doped soda-lime silicate and aluminosilicate glasses,” *Phys. Rev. B* **56**, 9302-9318 (1997).
 23. Z. Hu, Y. Wang, E. Ma, D. Chen, and F. Bao, “Microstructures and upconversion luminescence of Er³⁺ doped and Er³⁺/Yb³⁺ co-doped oxyfluoride glass ceramics,” *Mater. Chem. Phys.* **101**, 234-237 (2007).
 24. T. Wang, J. Zhou, S. Shi, B. Li, and R. Zong, “Preparation of size-controlled nanocrystalline infrared-to-visible upconverting phosphors Gd₂O₃: Yb, Er by using a water-in-oil micro-emulsion system,” *J. Electroceram.* **21**, 765-769 (2008).
 25. W. Lu, L. Cheng, H. Zhong, J. Sun, J. Wan, Y. Tian, and B. Chen, “Dependence of upconversion emission intensity on Yb³⁺ concentration in Er³⁺/Yb³⁺ co-doped flake shaped Y₂(MoO₄)₃ phosphors,” *J. Phys. D: Appl. Phys.* **43**, 085404 (2010).
 26. R. S. Yadav, R. K. Verma, A. Bahadur, S. B. Rai, “Structural characterizations and intense green upconversion emission in Yb³⁺, Pr³⁺ co-doped Y₂O₃ nano-phosphor,” *Spectrochim. Acta Part A* **137**, 357-362 (2015).
 27. S. Q. Man, H. L. Zhang, Y. L. Liu, J. X. Meng, E. Y. B. Pun, and P. S. Chung, “Energy transfer in Pr³⁺/Yb³⁺ codoped tellurite glasses,” *Opt. Mater.* **30**, 334-337 (2007).
 28. J. Cai, X. Wei, F. Hu, Z. Cao, L. Zhao, Y. Chen, C. Duan, and M. Yin, “Up-conversion luminescence and optical thermometry properties of transparent glassceramics containing CaF₂:Yb/Er nanocrystals,” *Ceram. Int.* **42**, 13990-13995 (2016).
 29. S. Haas, A. Hoell, R. Wurth, C. Rüssel, P. Boesecke, and U. Vainio, “Analysis of nanostructure and nanochemistry by SAXS: Accessing phase composition of oxyfluoride glass ceramics doped with Er³⁺/Yb³⁺,” *Phys. Rev. B* **81**, 184207 (2010).
 30. Y. C. Suling, Zhao, Zhiqin Liang, Meng Han, Zheng Xu, “Optimized upconversion emission of NaLuF₄:Er,Yb nanocrystals codoped with Gd³⁺ ions and its mechanism,” *J. Alloys Comp.* **593**, 30-33 (2014).
 31. Z. Liu, B. Mei, J. Song, and W. Li, “Fabrication and optical characterizations of Yb, Er codoped CaF₂ transparent ceramic,” *J. Eur. Ceram. Soc.* **34**, 4389-4394 (2014).
 32. L. A. Diaz-Torres, O. Meza, D. Solis, P. Salas, and E. D. Rosa, “Visible upconversion emission and non-radiative direct Yb³⁺ to Er³⁺ energy transfer processes in nanocrystalline ZrO₂:Yb³⁺, Er³⁺,” *Opt. Laser. Eng.* **49**, 703-708 (2011).